

This is the peer reviewed version of the following article:

Surface Reactivity of Ag-Modified Ceria to Hydrogen: A Combined Experimental and Theoretical Investigation / Benedetti, S.; Righi, G.; Luches, P.; D'Addato, S.; Magri, R.; Selloni, A.. - In: ACS APPLIED MATERIALS & INTERFACES. - ISSN 1944-8244. - 12:24(2020), pp. 27682-27690-27690. [10.1021/acsami.0c03968]

Terms of use:

The terms and conditions for the reuse of this version of the manuscript are specified in the publishing policy. For all terms of use and more information see the publisher's website.

18/12/2025 11:09

Surface reactivity of Ag-modified ceria to hydrogen: a combined experimental and theoretical investigation

Stefania Benedetti¹, Giulia Righi^{1,2,#}, Paola Luches¹, Sergio D'Addato^{1,2}, Rita Magri^{1,2,}, Annabella Selloni³*

¹CNR – Istituto Nanoscienze, via Campi 213/A, 41125 Modena, Italy

²Dipartimento di Fisica, Informatica e Matematica, Università di Modena e Reggio-Emilia, via Campi 213/A, 41125 Modena, Italy

³Department of Chemistry, Princeton University, New Jersey, 08540, United States

Keywords: ceria, metal dopants, hydrogen dissociation, X-ray photoemission spectroscopy, density functional theory, reaction kinetics, surface reduction, silver

Abstract

We investigate the mechanism of H₂ activation on Ag-modified cerium oxide surfaces, of interest for different catalytic applications. The study is performed on thin epitaxial cerium oxide films, investigated by X-ray photoemission spectroscopy to assess the changes of both the Ag oxidation state and the concentration of Ce³⁺ ions, O vacancies and hydroxyl groups on the surface during thermal reduction cycles in vacuum and under hydrogen exposure. The results are interpreted using density functional theory calculations to model pristine and Ag-modified ceria surfaces. Although the reactivity of ceria towards H₂ oxidation improves when a fraction of Ce cations is substituted with Ag, the concentration of reduced Ce³⁺ ions in Ag-modified ceria is found to be lower than in pure ceria under the same conditions. This behavior is observed even though the number of surface oxygen vacancies caused by the thermal treatment under hydrogen exposure is larger for the Ag-modified surface. These results are explained in terms of a change of the oxidation state of the surface Ag, which is able to acquire some of the extra surface electrons created by the oxygen vacancies and the adsorbed hydrogen atoms. Our findings provide new insights into the reactivity of Ag-modified ceria, which has been proposed as a promising alternative to platinum electrodes in electro-chemical devices.

Introduction

Recently, a wealth of research efforts has been devoted to the search of earth-abundant electrode materials that might replace platinum, the best-known catalyst currently employed in industrial applications. Among such materials reducible metal oxides have been found to have a high potential for many different applications, and, in particular, for catalytic reactions in electrochemical devices ¹.

Reducible oxides play an important role in heterogeneous catalysis due to their ability to store or release oxygen depending on the conditions of pressure and temperature.^{2 3} Among reducible oxides, CeO₂ has been suggested for a number of applications, from biomedicine⁴ to fuel cells (FC)^{5 6}. For example, motivated by the need to decrease the amount of Pt used in electrochemical devices, numerous studies have shown that Pt-modified CeO₂ is a promising electrode material for proton-exchange membrane FCs (PEMFCs), due to its high activity in mediating the formation of protons from gas-phase H₂⁶. In this context, it has been proposed that single atom catalysts can provide a viable route to further decrease the concentration of noble metal on the oxide surface⁷.

Ceria-based catalysts are of considerable interest also for hydrogenation reactions^{8 9}. Cerium oxide powder catalysts have been shown to be active towards H₂ dissociation, with an activity that depends on variables like the size and morphology of the catalysts and the density of defects and oxygen vacancies¹⁰. On the other hand, studies on model (111) ceria surfaces show that high temperatures and/or high pressures are required to dissociate H₂^{11 12}. On such surfaces the presence of oxygen vacancies favors H migration into the bulk¹², and temperature influences the steps that bring from H adsorption to ceria reduction.¹³

It is known that cation doping often improves the catalytic activity of metal oxides¹³. In ceria, cation dopants usually sit at substitutional cerium sites^{14 15}. In particular, Ag constitutes a low-valence dopant (LVD) in CeO₂ since in its stable oxides it has a lower valence than the Ce atoms in CeO₂. An interesting feature of LVD dopants is to make the neighboring oxygen atoms much more reactive¹³. Density functional theory (DFT) calculations on Ag single atoms on the CeO₂ (111) surface have indeed found that one oxygen in proximity of the Ag dopant can spontaneously leave the surface in an exothermic reaction^{16 17}. Since oxygen vacancies induce excess electrons that can reduce the oxidation state of Ce from 4+ to 3+ (with the extra electron occupying the localized *f* orbital), it is expected that the presence of Ag will ultimately lead to the creation of additional reduced cerium atoms on the CeO₂ surface^{18 19}.

More generally, experiments and calculations on ceria deposited on transition and noble metal supports or, vice versa, on metal nanoparticles deposited on a ceria support, have shown an increase of Ce³⁺ concentration as a consequence of the thin film/support interaction^{19 20 21 22 17 23 24}. Also doping with metals such as Cu and Rh has been reported to enhance the oxide reducibility^{25 26 27 28 29 17}. Higher concentrations of Ce³⁺ cations are often considered to be linked to a higher reactivity of the film to H₂ activation. In fact, DFT studies have shown that H₂ dissociation on pristine ceria surfaces leads to the formation of surface hydroxyl groups and the reduction of Ce⁴⁺ to Ce³⁺ cations^{30 31 32 33}. Moreover, a recent combined experimental and theoretical study found that isolated Pt²⁺ species on CeO₂ are inactive due to the large activation energy for breaking the H-H bond, and trace amounts of metallic Pt are necessary to initiate H₂ dissociation; this leads to the reduction of Ce⁴⁺ cations which, in turn, is coupled to the reduction of Pt²⁺ species.³⁴ As a result of these and

related studies, one of the experimental approaches for the study of H₂ dissociation on metal doped ceria films is to determine the oxidation states of both the dopant metal cation and the Ce cations using photoemission spectroscopy³⁴.

In the present study we provide new insights into the mechanisms of H₂ dissociation on Ag-modified ceria, with the aim to elucidate the role of Ag in the surface reactivity and its relation to the reduction of the Ce⁴⁺ cations. We will discuss in particular the validity of assessing the reactivity of the surface towards H₂ dissociation by monitoring the concentration of the Ce³⁺ reduced cations.

Methodology

Experiment

CeO₂ films were grown on Pt(111) single crystals, prepared by repeated cycles of Ar sputtering (1 keV, 1 μ A/cm²) and annealing (1040 K). The clean surface showed no impurities within the X-ray photoelectron spectroscopy (XPS) detection limit and a sharp (1x1) low energy electron diffraction pattern. CeO₂ films were grown by e-beam evaporation of Ce atoms in O₂ partial pressure of 1x10⁻⁷ mbar introduced through a nozzle. During the evaporation the substrate was kept at room temperature (RT). An evaporation rate of 0.4 Å/min was measured with a quartz microbalance before evaporation and the film thickness was checked by XPS after deposition. A film thickness of 1.5 nm corresponding to 5 ML was chosen. Ag-modified (Ag:CeO₂) films of the same thickness were obtained by co-deposition of Ag atoms by an effusion cell pointing towards the same position as the e-beam Ce evaporator, where the sample is placed. After deposition the films were annealed at 770 K in 1x10⁻⁷ mbar O₂ partial pressure in order to improve crystalline order and obtain full oxidation of the film. An Ag concentration of 10 at% was measured by XPS after the treatment.

Thermal cycles were performed by annealing either in ultra-high vacuum (UHV) (1x10⁻⁹ mbar) or in H₂ (1x10⁻⁷ mbar, 99.9995% purity) for 15 min at four different temperatures: 470 K, 570 K, 670 K and 770 K and cooling to RT in reducing atmosphere (UHV or H₂). In UHV conditions the residual H₂O partial pressure is 3x10⁻¹⁰ mbar. When H₂ is introduced in the chamber no change in H₂O partial pressure is observed. The XPS measurements were performed in UHV conditions at RT after each reduction step, exploiting an Al-K α X-ray source and a hemispherical analyzer (overall resolution 1 eV). The spectra were measured at grazing emission with respect to the sample surface (65° off-normal). The Ce 3d spectra were fit using five doublets - three related to Ce⁴⁺ ions and two related to Ce³⁺ ions -, following the procedure by Skala^{35 36} (see Supporting Information for details, Figure S1). The Ce³⁺ concentration is obtained from the fits by considering the ratio of the area of the two Ce³⁺ related doublets and the total area of the five doublets. The error on the concentration is estimated from the fits as $\pm 2\%$. Indeed, the accuracy of the absolute values obtained is possibly lower, due to the complexity of the spectra and of the background. Moreover, the true Ce³⁺ surface concentration is probably

systematically underestimated because of a partial sensitivity of XPS also to the deeper layers, which are not expected to be affected by reduction. However, the considerations made in this work are based only on the trends observed for the Ce³⁺ concentration with the temperature for the two different surfaces and in the two different environments and not on the absolute values of the concentration. The binding energy scale has been calibrated to have the Pt 4f peak at 71.2 eV. The O 1s spectra were fit by the sum of two Voigt-shaped peaks with the same width, fixed binding energies, and using their intensities as a fitting parameter. The Ag 3d peaks were fit by a Doniach-Sunjich doublet to determine their binding energy.

Scanning tunneling microscopy (STM) was used to check for possible modifications of surface morphology induced by doping and/or by the thermal treatments. The STM images were acquired at RT with an Omicron RT AFM/STM using a W tip in constant current mode and with a positive sample-to-tip bias. The images were processed using WSxM software³⁷.

Density Functional Theory calculations

We performed ab-initio spin-polarized calculations using the Perdew-Burke-Ernzerhof (PBE)³⁸ exchange and correlation functional as implemented in the Quantum Espresso package^{39 40}. Ultrasoft pseudopotentials⁴¹ were employed to describe the interaction between electrons and ions. The wave function and charge density cutoff were set to 30 Ry and 240 Ry, respectively. To treat the strongly correlated electrons in the f orbitals of Ce atoms we have used the Hubbard Correction (DFT+U), as implemented by Cococcioni.⁴² We have set the U value to 4 eV, as used previously^{16 24}.

CeO₂ crystallizes in the fluorite structure. Optimizing the primitive cell using a (7x7x7) Monkhorst-Pack⁴³ grid we obtained an equilibrium lattice parameter $a = 5.52 \text{ \AA}$, in reasonable agreement with the experimental value, $a_{\text{exp}} = 5.41 \text{ \AA}$ ⁴⁴, and previous theoretical studies^{45 46}.

To describe the surface, we used a (111) slab with a (4x4) surface supercell and three O-Ce-O trilayers. The periodically repeated slabs were separated by 15 Å of vacuum. The positions of the atoms in the last trilayer were kept fixed to their bulk positions during the geometry optimization. The energy convergence threshold for the geometric optimizations was set to 10⁻⁵ eV. We relaxed the structure until the forces on the atoms of the slab were less than 0.01 eV/Å. The Brillouin zone was sampled only at the Gamma point. The O₂ molecule was relaxed in a box with a 20 Å edge.

We calculated the Oxygen vacancy formation energy E_{form} as: $E_{\text{form}} = E_{\text{def}} + 1/2 E_{\text{O}_2} - E_{\text{pristine}}$, where E_{def} is the energy of the slab with one surface Oxygen vacancy, E_{O_2} is the energy of the Oxygen molecule, and E_{pristine} is the energy of the slab without the Oxygen vacancy.

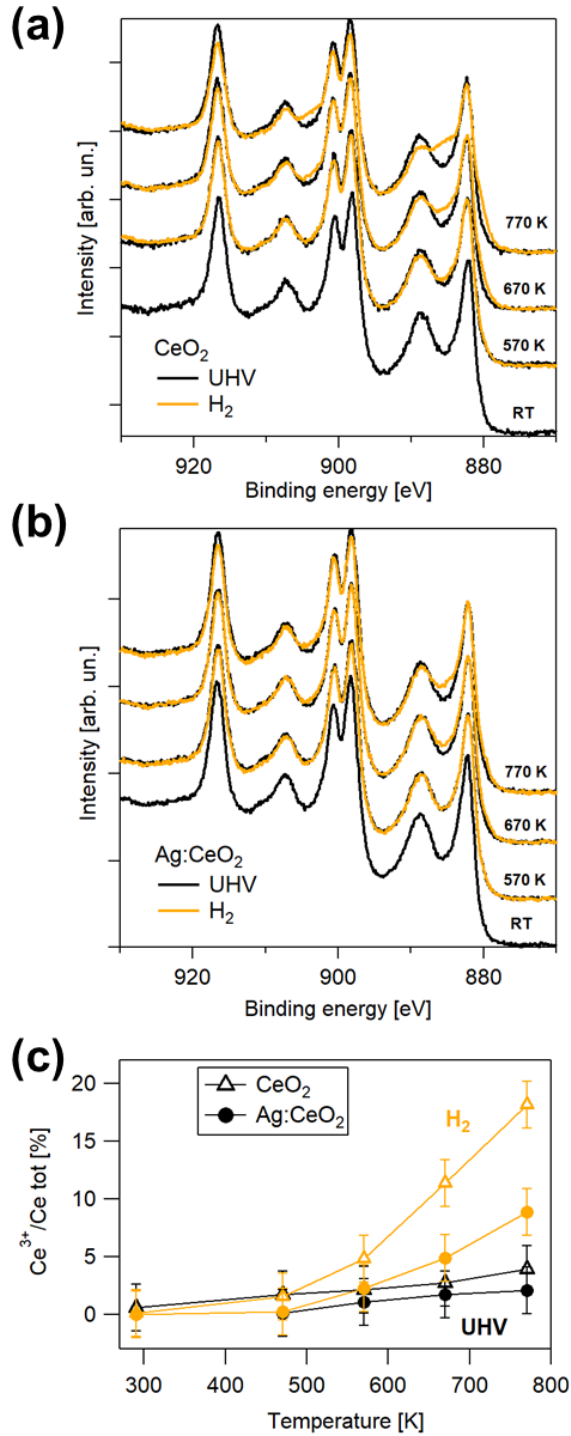


Figure 1. Ce 3d spectra for (a) pure and (b) Ag-modified CeO₂ film reduced at increasing temperature in UHV (black) and H₂ partial pressure (orange). (c) Ce³⁺ concentration as a function of temperature for the different films and reducing conditions, obtained from the fit of the Ce 3d spectra in panel (a) and (b).

To model the Ag-modified surfaces, we considered an Ag atom substituting one of the Ce atoms of the first monolayer, where the dopant effect on the surface reactivity is expected to be most important. This specific configuration is suggested by experimental results showing that noble metals such as Au and Pt tend to occupy cation positions^{14 15 47}. We focused on the (111) surface of ceria, which is the one exposed in our experiments, and, in particular, the stable surface with one oxygen vacancy near the Ag ion¹⁶.

To determine the minimum energy paths (MEP) of H₂ dissociation on the Ag:CeO₂ surfaces we have used the climbing image nudged method (CI-NEB)⁴⁸ with seven images. The obtained activation energies have been compared with the energy required to oxidize the H₂ molecule on the pristine ceria surface calculated in previous works^{32 49 31} using the same methodology. Charge transfers were calculated using the Bader approach⁵⁰.

Results and Discussion

EXPERIMENT

• Evolution of Ce³⁺ concentration

To understand the role of Ag atoms in CeO₂ we have investigated the changes induced by thermal cycles in reducing environments in a 5 ML pure CeO₂ film and in a film of the same thickness with substitutional Ag atoms. During the thermal cycle the film was exposed to the reducing environment (either UHV or H₂) both during the annealing and the cooling to RT. The evolution of the Ce³⁺ concentration and the surface modifications in the film have been investigated by means of XPS and STM.

Figure 1a compares the Ce 3d spectra of the pure CeO₂ film after the temperature treatment in H₂ and, for comparison, in UHV in order to rule out the possible effects coming from the residual gas in the chamber. At RT the lineshape is consistent with the presence of Ce⁴⁺ ions only. It can be observed that the increase of the annealing temperature induces negligible variations in the lineshape under UHV conditions, while the annealing and the subsequent cooling in H₂ modifies more significantly the Ce 3d spectra, which show a relevant contribution from Ce³⁺ ions above 670 K. The observed reduction is less pronounced at normal emission, showing that the process occurs mainly at the surface (see Supporting Information, Figure S2).

When 10 at% of Ag atoms are added to the oxide matrix the trend is the same and annealing in H₂ induces a larger reduction as compared to UHV treatments above 670 K (Figure 1b). A fit of the Ce 3d spectra was performed to quantify the concentration of Ce³⁺ and Ce⁴⁺ in the two samples under the different treatments. The fits of the curves are reported in the Supporting Information (Figure S3 and Table S1). Figure 1c shows the Ce³⁺ concentration as determined by the fit for the two samples after the different reducing steps in UHV and in H₂. The UHV treatment brings to a maximum Ce³⁺ concentration of about 4% in pure CeO₂ and 2% in Ag:CeO₂. Annealing in H₂ induces a non-negligible reduction in the pure oxide already at 470 K, while for Ag:CeO₂ the Ce³⁺ concentration starts to increase at 570 K. In general, the Ce³⁺ concentration is larger in the presence of H₂ and it is significantly higher for the pure (18%) as compared to the Ag:CeO₂ (9%) film at 770 K.

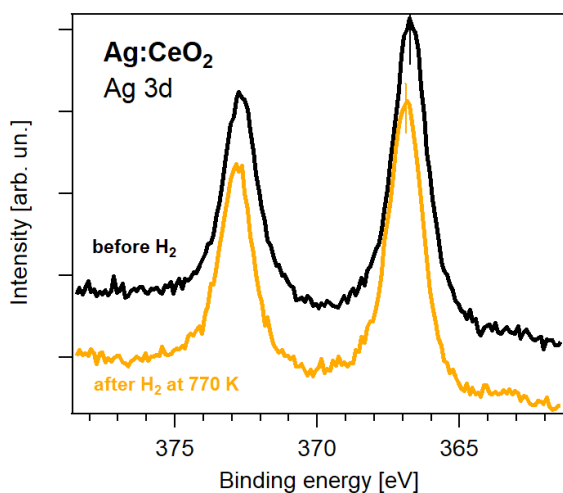


Figure 2: Ag 3d peaks of the Ag-modified CeO₂ film before (black curve) and after (orange curve) H₂ exposure at 770 K.

The Ag 3d XPS lines were also measured at each step of the different thermal treatments in UHV and H₂ for the Ag:CeO₂ sample (Figure 2). The spectra do not show any significant change in shape, width or intensity with the thermal treatments, showing a stable distribution of Ag in the matrix. A small binding energy shift is revealed after the film is treated in hydrogen. The Ag 3d_{5/2} binding energy is 367.8 eV before the H₂ thermal treatment, while it shifts to 368.0 eV afterwards. Ag 3d_{5/2} in metallic silver has a binding energy of 368.2 eV⁵¹, while it was shown that in its oxides an anomalous negative shift to lower binding energy occurs, because of extra-

atomic relaxation effects⁵². The data therefore show that Ag atoms in the ceria matrix are in an oxidized state and that the exposure to hydrogen partially reduces them, in accordance with theoretical predictions (see below). It is difficult to estimate the oxidation state from the absolute values of the binding energies. The value obtained before H₂ reduction in fact corresponds to the literature one for Ag¹⁺. However, previous

studies have shown that the binding energies of metal cations in their bulk oxides can be different from those of the same cations with the same oxidation state introduced as low-concentration dopants in a matrix of a different oxide ⁵³.

- **Formation of surface oxygen vacancies and OH groups**

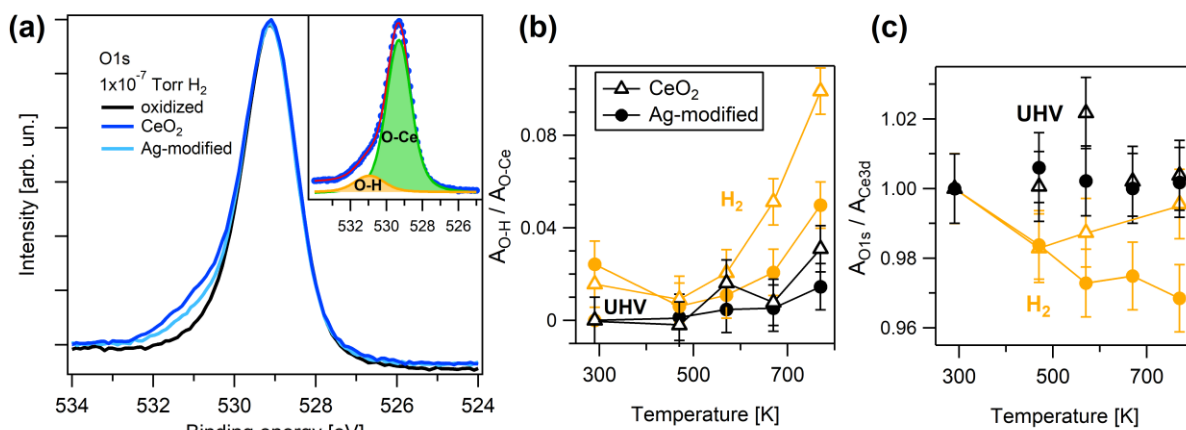


Figure 3. (a) O1s peaks of pure and Ag:CeO₂ films before and after exposure to H₂ at 770 K. Inset shows the Voigt peaks used for the fit of the pure CeO₂ after exposure to H₂. (b) Ratio between H-coordinated O and Ce-coordinated O peaks after H₂ (orange) and UHV (black) exposure (as obtained by the fit) as a function of temperature. (c) Ratio between O 1s and Ce 3d peak area after H₂ exposure or UHV treatment at different temperatures.

During the thermal treatment in hydrogen, we also observed non-negligible modifications in the O 1s peak (Figure 3) in parallel to the modifications of the Ce 3d peak. Increasing the temperature during H₂ reduction a component appears at about 1.7 eV higher binding energy with respect to the main peak (Fig. 3a). A quantitative estimation of the intensity of the new component is obtained through a fit with two Voigt peaks, a dominant one centered at 529.3 eV, assigned to O in cerium oxide lattice, and a small peak at 531 eV, related to O coordinated to H ^{54 55 56}. An example of the resulting fit is reported in the inset of Figure 3a. Figure 3b shows the ratio between the peaks of the OH component and the O-Ce main component. The weight of the OH component is slightly higher for the Ag:CeO₂ film after H₂ exposure at RT, while it becomes significantly higher for the pure oxide after exposure at higher temperatures. The OH-related intensity is higher at grazing emission than at normal emission, showing that the OH species are preferentially located at the surface (see Supporting Information, Figure S2).

The spectra of Figure 3a do not show any measurable peak at the binding energies where peaks from adsorbed water are expected, i.e. at approximately 533.5 eV ^{54 55 56}. Water does actually form, but it is released from the surface at high temperatures leaving O vacancies. Moreover, the ceria surfaces reduced by thermal treatment in H₂ have a low propensity towards adsorption of molecular water during their cooling to RT in hydrogen ⁵⁶.

Figure 3c reports the ratio of the O 1s to Ce 3d areas after the different thermal treatment steps in H₂ and UHV for the pure and the Ag:CeO₂ films. The ratio is approximately constant for both samples in UHV, in agreement with the negligible changes observed in the Ce 3d lineshapes. In H₂ environment, a more pronounced decrease of the ratio in the Ag:CeO₂ film as compared to the pure oxide film as a function of temperature is observed. This is related to the formation of a higher concentration of oxygen vacancies, and it can be very likely ascribed to a more efficient water formation on the Ag-modified surface.

- **Surface morphology**

To exclude possible contributions coming from differences in surface morphology or from uncovered substrate areas, we compare the STM images of the CeO₂ film with and without Ag inclusion. Figure 4a reports the STM image of the CeO₂ film after the initial oxidation at 770 K, showing that the film completely covers the Pt surface with grains of about 5 nm diameter. The morphology of the film with Ag inclusion is not significantly different from that of the pristine film (Figure 4b) and it is not modified after thermal treatments in H₂ (see Supporting Information, Figure S4). Figure 4c shows two height profiles across the darkest areas observed on the film surfaces. For both films the average hole depth is about 1 nm (dashed line), well below the estimated film thickness of 1.56 nm (5 ML). The hole depth may be underestimated due to tip size effects, which have not been removed due to an unknown tip size. However, since the dark holes represent a very small surface fraction, similar for both pristine and Ag:CeO₂ surfaces, they are not expected to significantly influence the surface chemical activity observed so far.

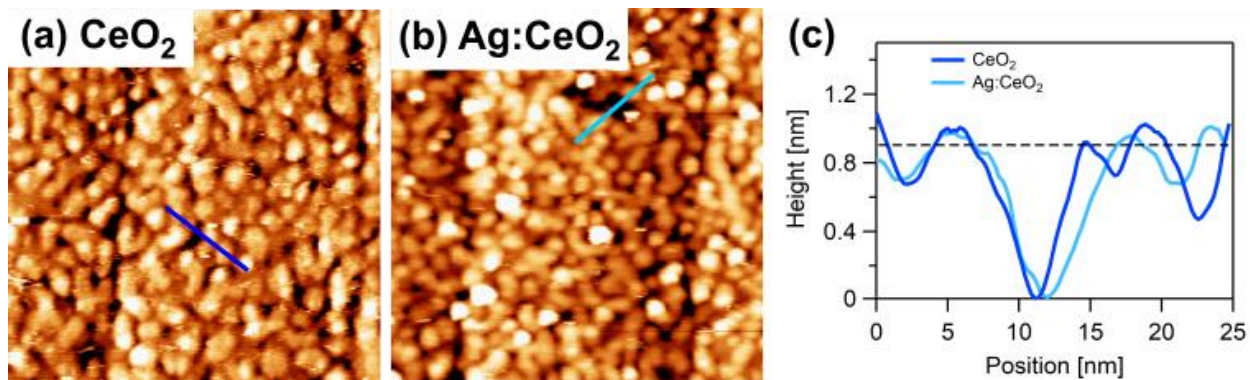


Figure 4. 100x100 nm² STM images of 5 ML (1.56 nm) (a) pure CeO₂ and (b) Ag:CeO₂ film, annealed at 770 K in O₂ (U = 2.5 V, I = 0.08 nA). (c) Height profiles along the lines in images (a) and (b).

THEORY

To obtain more detailed insight into our experimental observations, we further examined the reduction of the pristine and Ag-doped ceria surfaces under UHV conditions and in a H_2 environment using DFT calculations. Side and top views of the pristine and Ag:CeO₂ (111) surface models investigated in this work are shown in Figure 5.

- **Reduction in vacuum**

Reducible oxides under UHV conditions tend to lose oxygen with increasing temperature. To characterize this process, we have calculated the energy required to create one oxygen vacancy (O_v) on the pristine and Ag:CeO₂(111) surfaces. On pristine ceria (Figure 5a,b) the O_v formation energy is $E_{form} = 2.02$ eV, a value close to those reported in previous theoretical works^{57,58}. Following the creation of the oxygen vacancy we observe the reduction of two Ce atoms on second neighbor sites of the O_v .

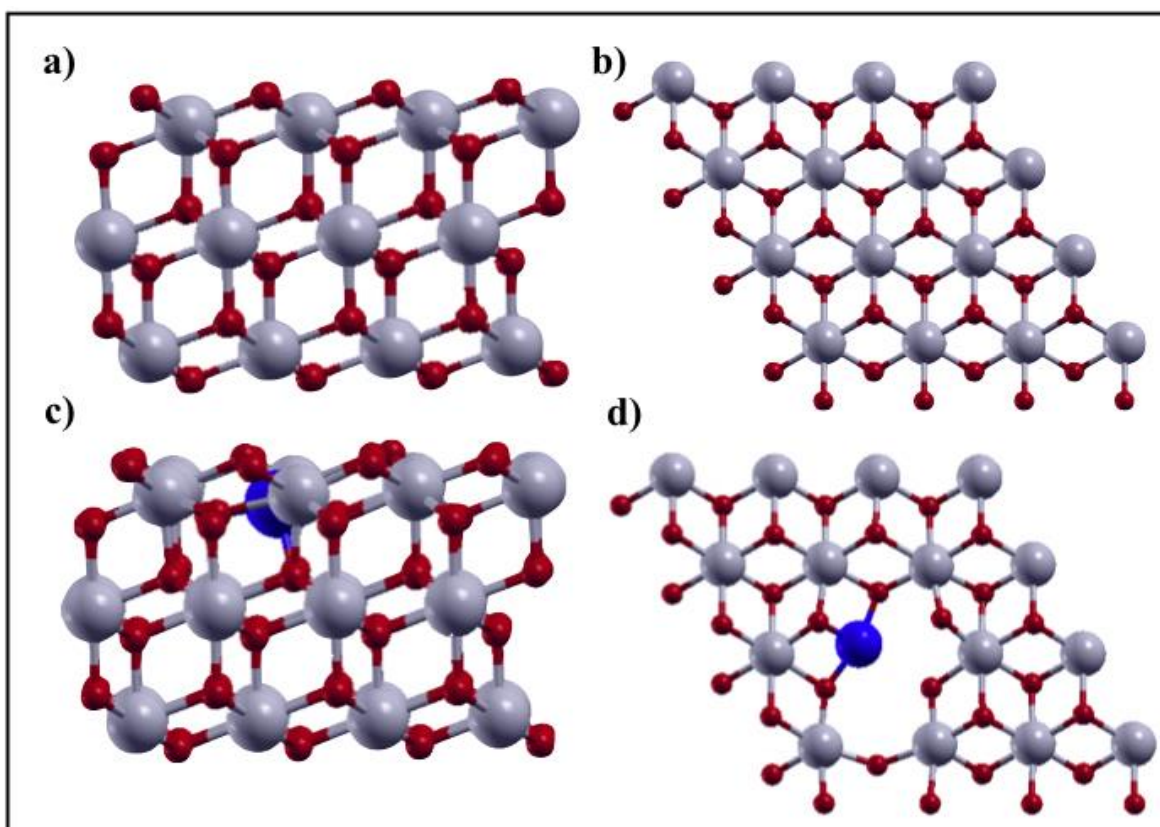


Figure 5. Side (a,c) and top (b,d) views of the different surface configurations. a) and b) CeO₂ surface; c) and d) Ag:CeO₂ surface. Gray, red and blue balls are the cerium, oxygen and silver atoms, respectively.

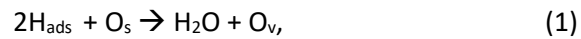
We modeled the Ag:CeO₂ surface by substituting one Ce atom per surface unit cell with Ag. The oxygen ions near the Ag atom are less negatively charged than on the pristine ceria (≈ -0.2 e), and are also more active

than the other surface oxygen atoms⁵⁹. The removal of one of such oxygens is a thermodynamically favored process with $E_{\text{form}} = -0.76$ eV. This implies that the most stable surface actually contains dopant-vacancy complexes, as shown in Figure 5c and d. On this surface, the Ag oxidation state is 2+, and the energy required to remove an additional oxygen atom close to Ag is positive, 0.78 eV, but still lower than on pristine CeO₂. Creation of such an additional O_v reduces the Ag oxidation state from 2+ to 1+, while at the same time one surface Ce atom is reduced to Ce³⁺. Altogether, we can conclude that the formation of an oxygen vacancy on the Ag-modified surface causes the reduction of only one Ce atom, whereas two Ce atoms are reduced on the pristine surface. These results indicate that loss of surface oxygen due to thermal treatment under UHV conditions causes the creation of more Ce³⁺ cations in pure ceria than in Ag-modified ceria, consistent with the experimental data (Fig. 1c).

- **Reduction in H₂ atmosphere**

In H₂ environment, both hydrogen adsorption and the formation of oxygen vacancies contribute to the surface reduction. As shown by recent computational studies, the dissociative adsorption of H₂ has an activation energy $E_a = 0.99$ eV and leads to the reduction of two Ce ions on the pristine surface^{32,31}, whereas the barrier is much lower, 0.34 eV, on Ag:CeO₂, where one Ce ion and one Ag are reduced¹⁶. These results suggest that the hydrogen coverage should be higher on Ag:CeO₂ than on the pristine surface at low temperature, whereas the fraction of Ce³⁺ ions should be higher on the pristine surface, a result consistent with the experimental data in Figs. 1c and 3b. These results are also compatible with the decrease of Ag oxidation state observed by XPS after H₂ exposure at high temperature (Figure 2).

Under conditions of high temperature and low water pressure, adsorbed hydrogen (H_{ads}) on reducible metal oxides can undergo the reaction



where O_s and O_v denote a surface oxygen atom and surface oxygen vacancy, respectively. Temperature programmed reduction measurements acquired by several groups on cerium oxide powdered catalysts indicate that adsorbed hydrogen can indeed be released from the surface in the form of H₂O forming O vacancies on the surface at around 770 K, while the formation of bulk oxygen vacancies requires a temperature of 1100 K.^{8,10}

Table 1 - Relative free energies (in eV) of non-interacting gas phase H₂ and surface (H₂(g) + surface), surface with adsorbed hydrogen (2H_{ads}), and reduced surface with a desorbed gas phase water molecule (H₂O(g) + O_v) at different temperatures. The energy of the 2H_{ads} state is taken as the reference. Values in bold are computed at the low pressure of the experiment ($p_{\text{H}_2} = 10^{-10}$ bar), those in parentheses refer to the standard pressure ($p^0 = 1$ bar). Reported values include zero-point energy corrections of gas phase and adsorbed species and entropic

contributions to the free energy of gas phase molecules only. Water formation (H_2 adsorption) is much more (less) exothermic at low pressure.

Surface Type	State	T= 0K	T= 300 K	T=400 K	T=500 K	T = 600 K
CeO ₂	H ₂ (g) + surf	2.05	1.14 (1.73)	0.80 (1.59)	0.46 (1.44)	0.11 (1.29)
	2H _{ads}	0.00	0.00	0.00	0.00	0.00
	H ₂ O(g)+ O _v	0.89	-0.18 (0.41)	-0.59 (0.20)	-0.99 (-0.01)	-1.40 (-0.22)
Ag:CeO ₂	H ₂ (g) + surf	2.38	1.47 (2.06)	1.13 (1.92)	0.79 (1.77)	0.44 (1.62)
	2H _{ads}	0.00	0.00	0.00	0.00	0.00
	H ₂ O(g)+ O _v	0.75	-0.32 (0.27)	-0.73 (0.06)	-1.13 (-0.15)	-1.54 (-0.36)

The computed relative free energies of the reactant and product states of (1) on the pristine and Ag-doped CeO₂ surface are reported in Table 1 for several temperatures between zero and 600 K. As expected, the adsorption of H₂ becomes increasingly less exothermic with increasing temperature, while the reverse is true for the formation of a water molecule from two adsorbed H and a surface oxygen atom. At the low pressure of our experiment, in particular, water formation is (slightly) exothermic already at room temperature and leads to a free energy gain even larger than that of H₂ adsorption above ~ 450 K.

As a plausible pathway for reaction (1), we assume that water formation is due to the diffusion of one H_{ads} to another surface OH_{ads} group with which it recombines. Diffusion of H into the bulk could be another possible pathway for the hydrogen atoms, but it would not account for the observed trends since it would lead to the reduction of the surface O-H without changing the surface O content. Our calculated Minimum Energy Pathways for reaction (1) on the pristine and Ag-doped surfaces are shown in Fig. 6. To estimate the barrier for H diffusion, we follow Fernández-Torre.³⁰, who found that a H atom on CeO₂(111) first diffuses from O_s (Initial state IS) to a subsurface oxygen (O_{sub}), reaching a metastable state (MS). For pristine CeO₂, our computed energy barrier for H diffusion from a surface to a subsurface oxygen (IS→MS) is 1.13 eV, while it is 0.77 eV for Ag:CeO₂. The computed barrier for H₂O desorption (the finale state FS) is in both cases lower than the H diffusion barrier, indicating that H diffusion is the rate limiting process for water formation on both surfaces. The lower H-diffusion barrier on the Ag:CeO₂ surface thus suggests that water is more likely to form on Ag-modified than on pristine CeO₂.

The results of our calculations allow us to explain the observed trends in the surface concentration of OH, shown in Figure 3b, which increases with the RT exposure of the film to H₂, slightly decreases at 470 K and significantly increases above 570 K. The increase at RT after H₂ exposure is related to H₂ adsorption and dissociation, which are predicted to have activation barriers of 0.99 and 0.34 eV on the pristine and Ag-doped

surfaces respectively, consistent with the observed larger concentration on the latter. As the temperature is increased to 470 K, water formation and desorption become important, leading to a decrease of both surface O and OH concentrations. At higher temperature the annealing and subsequent cooling of the film in H₂ induces further hydrogen dissociation and a consequent increase of the concentration of OH bonds. H preferentially binds to oxygen atoms, which have a higher concentration on the pristine ceria than on the Ag-modified surface, explaining the higher OH concentration on the former after the treatment at high temperatures. Also the significant decrease in O/Ce ratio shown in Figure 3c for the Ag:CeO₂ indicates a higher concentration of oxygen vacancies on the Ag-modified surface, which is likely due to a more efficient water formation on this surface, as predicted by the DFT results. Furthermore, the larger concentration of surface OH groups on the pristine surface than on Ag:CeO₂ possibly contributes to the much larger concentration of Ce³⁺ ions experimentally observed on pristine CeO₂ than on Ag:CeO₂ after hydrogen exposure, reported in Fig. 1c.

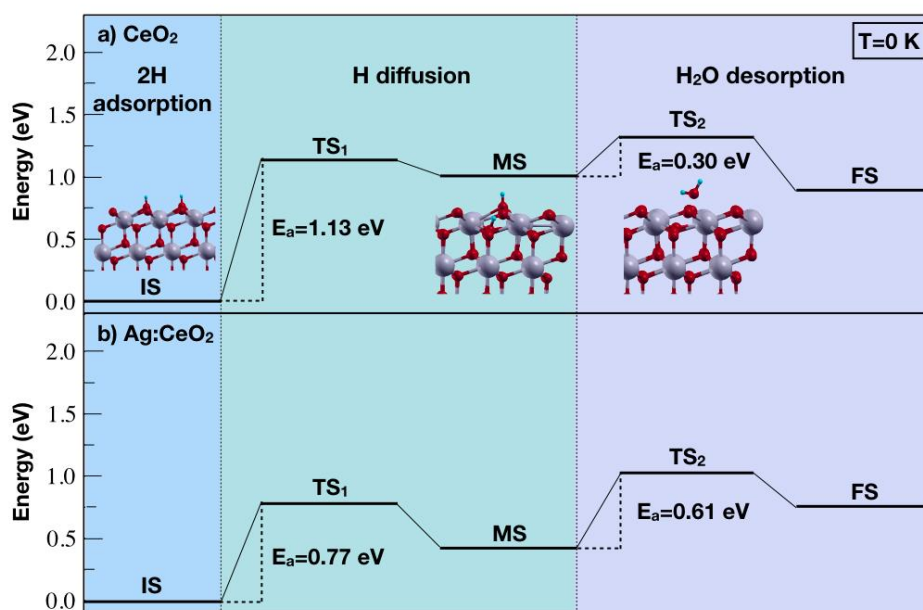


Fig. 6 Minimum Energy Path (MEP) of reaction (1) on the a) CeO₂ and b) Ag:CeO₂ surface at T=0K. The energy zero corresponds to the surface with dissociatively adsorbed H₂. Grey balls indicate cerium atoms, red balls oxygen atoms, and the small light blue balls the hydrogen atoms.

Conclusions

In this work we aimed to obtain insight into the reactivity of Ag-modified ceria films towards H₂ by investigating the changes occurring on the film surface after thermal treatments in vacuum and in hydrogen

partial pressure. As expected, the H₂ environment induces a significantly higher Ce³⁺ concentration as compared to reduction in vacuum at the same temperatures. Quite surprisingly, however, the Ag-modified sample showed a lower concentration of Ce³⁺ cations than the pristine ceria one under all conditions, also in the presence of a greater number of oxygen vacancies. To interpret these results, we carried out DFT calculations and found that the presence of Ag reduces the barrier of H₂ dissociation on the ceria surface, explaining the larger concentration of OH groups on the Ag-modified surface at low temperature, as observed experimentally. Our calculations also show that doping with Ag decreases the activation barrier for surface diffusion of adsorbed H atoms, which is the rate limiting process for water formation, thus suggesting a larger rate of water formation on the Ag-modified than on the pristine samples at high temperature. This prediction is confirmed by the higher concentration of surface oxygen vacancies and lower concentration of OH groups on the Ag:CeO₂ surface found in the experiments. Both H₂ dissociative adsorption and oxygen vacancies contribute to the creation of Ce³⁺ cations, but in both cases the number of reduced Ce cations is predicted to be two times larger on the pristine ceria surface relative to the Ag-modified one, in agreement with the experiment.

Our analysis shows that while measuring the amount of reduced Ce³⁺ cations often provides a reliable estimate of the CeO₂ surface activity towards oxidation reactions, this is not the case for Ag-modified CeO₂. Due to the tendency of Ag to compete with Ce in the acquisition of part of the surface electrons made available by hydrogen adsorption and oxygen vacancy formation, the concentration of Ce³⁺ cations remains relatively low even if the surface reactivity to hydrogen is enhanced.

Altogether, these results provide new insights into the mechanism of H₂ activation on CeO₂-based materials that could help the development of efficient Pt-free electrode materials for electro-chemical devices.

ASSOCIATED CONTENT

Supporting Information

Figure S1: Fit of Ce 3d spectra from CeO₂ film on Pt reduced at 770 K in H₂, performed following the well-established procedure described by Skála, T.^{35 36}. The figure shows the five doublets (blue for Ce³⁺, light blue for Ce⁴⁺) and the Shirley background.

Figure S2: (a) Ce 3d and (b) O 1s on pristine CeO₂ annealed at 770 K in H₂ measured at normal (red) and grazing (black) emission. The Ce³⁺ contribution in the Ce 3d and of the O-H contribution in the O 1s spectra are more intense at grazing emission, demonstrating that the investigated processes take place primarily at the surface.

Figure S3: Ce 3d spectra for 5 ML of pure CeO₂ in (a) UHV and (b) H₂ and Ag-modified CeO₂ (c-d) in the same environments. Red curves are the fits performed following the procedure reported by Skála, et al.^{35 36} as described in Figure S1.

Table S1: Ce³⁺ concentration obtained by the fitting procedure described in Figure S1 and reported in Figure 1 for the pure CeO₂ and Ag-modified films after annealing in UHV and H₂.

Figure S4: 100x100 nm² STM images of 5 ML (1.56 nm) Ag-modified CeO₂ film: (a) oxidized at 770 K in O₂ and (b) annealed at 770 K in H₂ (U = 2.5 V, I = 0.08 nA). Images show that the exposure to H₂ at high temperature does not induce significant modifications in the film morphology.

AUTHOR INFORMATION

Corresponding Author

* E-mail: rita.magri@unimore.it

Present Address:

[#]G. R.: Istituto Officina dei Materiali (IOM) c/o Scuola Internazionale Superiore di Studi Avanzati (SISSA), Via Bonomea 265, 43136 Trieste, Italy

Acknowledgements

The authors wish to thank Sergio Valeri for his support and for fruitful discussions. The work is performed with the financial support of Università degli Studi di Modena e Reggio Emilia through the FAR2016 project titled: “Innovative (oxide-based) materials and methods for fuel cell electrodes implementation”. Financial support from MIUR through PRIN project no. 2015CL3APH is also acknowledged. A.S. acknowledges support from DoE-BES, Division of Chemical Sciences, Geosciences and Biosciences under Award DESC0007347. We also acknowledge use of computational resources at the TIGRESS high performance computer center at Princeton University.

REFERENCES

- (1) Montini, T.; Melchionna, M.; Monai, M.; Fornasiero, P. Fundamentals and Catalytic Applications of CeO₂-Based Materials. *Chemical Reviews* **2016**, *116* (10), 5987–6041. <https://doi.org/10.1021/acs.chemrev.5b00603>.
- (2) Trovarelli, A.; Fornasiero, P. *Catalysis by Ceria and Related Materials*; World Scientific, 2013; Vol.

12.

- (3) Trovarelli, A.; Leitenburg, C. de; Boaro, M.; Dolcetti, G. The Utilization of Ceria in Industrial Catalysis. *Catalysis Today* **1999**, *50* (2), 353–367. [https://doi.org/10.1016/S0920-5861\(98\)00515-X](https://doi.org/10.1016/S0920-5861(98)00515-X).
- (4) Celardo, I.; Pedersen, J. Z.; Traversa, E.; Ghibelli, L. Pharmacological Potential of Cerium Oxide Nanoparticles. *Nanoscale* **2011**, *3* (4), 1411–1420. <https://doi.org/10.1039/C0NR00875C>.
- (5) Fiala, R.; Figueroba, A.; Bruix, A.; Vaclavu, M.; Rednyk, A.; Khalakhan, I.; Vorokhta, M.; Lavkova, J.; Illas, F.; Potin, V.; Matolinova, I.; Neyman, K. M.; Matolin, V. High Efficiency of Pt²⁺-CeO₂ Novel Thin Film Catalyst as Anode for Proton Exchange Membrane Fuel Cells. *Applied Catalysis B: Environmental* **2016**, *197*, 262–270. <https://doi.org/10.1016/j.apcatb.2016.02.036>.
- (6) Fiala, R.; Vaclavu, M.; Rednyk, A.; Khalakhan, I.; Vorokhta, M.; Lavkova, J.; Potin, V.; Matolinova, I.; Matolin, V. Pt–CeO_x Thin Film Catalysts for PEMFC. *Catalysis Today* **2015**, *240*, 236–241. <https://doi.org/10.1016/j.cattod.2014.03.069>.
- (7) Lykhach, Y.; Bruix, A.; Fabris, S.; Potin, V.; Matolínová, I.; Matolín, V.; Libuda, J.; Neyman, K. M. Oxide-Based Nanomaterials for Fuel Cell Catalysis: The Interplay between Supported Single Pt Atoms and Particles. *Catalysis Science & Technology* **2017**, *7* (19), 4315–4345. <https://doi.org/10.1039/C7CY00710H>.
- (8) Vilé, G.; Bridier, B.; Wichert, J.; Pérez-Ramírez, J. Ceria in Hydrogenation Catalysis: High Selectivity in the Conversion of Alkynes to Olefins. *Angewandte Chemie International Edition* **2012**, *51* (34), 8620–8623. <https://doi.org/10.1002/anie.201203675>.
- (9) Vilé, G.; Colussi, S.; Krumeich, F.; Trovarelli, A.; Pérez-Ramírez, J. Opposite Face Sensitivity of CeO₂ in Hydrogenation and Oxidation Catalysis. *Angewandte Chemie International Edition* **2014**, *53* (45), 12069–12072. <https://doi.org/10.1002/anie.201406637>.
- (10) Aneggi, E.; Boaro, M.; Leitenburg, C. de; Dolcetti, G.; Trovarelli, A. Insights into the Redox Properties of Ceria-Based Oxides and Their Implications in Catalysis. *Journal of Alloys and Compounds* **2006**, *408–412*, 1096–1102. <https://doi.org/10.1016/j.jallcom.2004.12.113>.
- (11) Höcker, J.; Menteş, T. O.; Sala, A.; Locatelli, A.; Schmidt, T.; Falta, J.; Senanayake, S. D.; Flege, J. I. Unraveling the Dynamic Nanoscale Reducibility (Ce⁴⁺ → Ce³⁺) of CeO_x–Ru in Hydrogen Activation. *Advanced Materials Interfaces* **2015**, *2* (18), 1500314. <https://doi.org/10.1002/admi.201500314>.
- (12) Werner, K.; Weng, X.; Calaza, F.; Sterrer, M.; Kropp, T.; Paier, J.; Sauer, J.; Wilde, M.; Fukutani, K.; Shaikhutdinov, S.; Freund, H.-J. Toward an Understanding of Selective Alkyne Hydrogenation on Ceria: On the Impact of O Vacancies on H₂ Interaction with CeO₂(111). *J. Am. Chem. Soc.* **2017**, *139* (48), 17608–17616. <https://doi.org/10.1021/jacs.7b10021>.
- (13) McFarland, E. W.; Metiu, H. Catalysis by Doped Oxides. *Chemical reviews* **2013**, *113* (6), 4391–4427. <https://doi.org/10.1021/cr300418s>.
- (14) Liu, J. Catalysis by Supported Single Metal Atoms. *Acs Catalysis* **2016**, *7* (1), 34–59. <https://doi.org/10.1021/acscatal.6b01534>.
- (15) Qiao, B.; Liu, J.; Wang, Y.-G.; Lin, Q.; Liu, X.; Wang, A.; Li, J.; Zhang, T.; Liu, J. Highly Efficient Catalysis of Preferential Oxidation of CO in H₂-Rich Stream by Gold Single-Atom Catalysts. *ACS Catalysis* **2015**, *5* (11), 6249–6254. <https://doi.org/10.1021/acscatal.5b01114>.
- (16) Righi, G.; Magri, R.; Selloni, A. H₂ Dissociation on Noble Metal Single Atom Catalysts Adsorbed

on and Doped into CeO₂ (111). *J. Phys. Chem. C* **2019**, *123* (15), 9875–9883.
<https://doi.org/10.1021/acs.jpcc.9b00609>.

(17) Gasperi, G.; Brugnoli, L.; Pedone, A.; Menziani, M. C.; Valeri, S.; Luches, P. Reducibility of Ag- and Cu-Modified Ultrathin Epitaxial Cerium Oxide Films. *J. Phys. Chem. C* **2019**.
<https://doi.org/10.1021/acs.jpcc.9b02378>.

(18) Tang, Y.; Zhang, H.; Cui, L.; Ouyang, C.; Shi, S.; Tang, W.; Li, H.; Chen, L. Electronic States of Metal (Cu, Ag, Au) Atom on CeO₂ (1 1 1) Surface: The Role of Local Structural Distortion. *Journal of Power Sources* **2012**, *197*, 28–37. <https://doi.org/10.1016/j.jpowsour.2011.09.026>.

(19) Luches, P.; Pagliuca, F.; Valeri, S. Structural and Morphological Modifications of Thermally Reduced Cerium Oxide Ultrathin Epitaxial Films on Pt(111). *Phys. Chem. Chem. Phys.* **2014**, *16* (35), 18848–18857. <https://doi.org/10.1039/C4CP02723J>.

(20) Luches, P.; Pagliuca, F.; Valeri, S.; Illas, F.; Preda, G.; Pacchioni, G. Nature of Ag Islands and Nanoparticles on the CeO₂(111) Surface. *The Journal of Physical Chemistry C* **2012**, *116* (1), 1122–1132. <https://doi.org/10.1021/jp210241c>.

(21) Szabová, L.; Stetsovych, O.; Dvořák, F.; Farnesi Camellone, M.; Fabris, S.; Mysliveček, J.; Matolín, V. Distinct Physicochemical Properties of the First Ceria Monolayer on Cu(111). *J. Phys. Chem. C* **2012**, *116* (11), 6677–6684. <https://doi.org/10.1021/jp211955v>.

(22) Pan, Y.; Nilius, N.; Freund, H.-J.; Paier, J.; Penschke, C.; Sauer, J. Titration of Ce³⁺ Ions in the CeO₂(111) Surface by Au Adatoms. *Phys. Rev. Lett.* **2013**, *111* (20), 206101.
<https://doi.org/10.1103/PhysRevLett.111.206101>.

(23) Brugnoli, L.; Pedone, A.; Menziani, M. C.; Adamo, C.; Labat, F. H₂ Dissociation and Water Evolution on Silver-Decorated CeO₂(111): A Hybrid Density Functional Theory Investigation. *J. Phys. Chem. C* **2019**, *123* (42), 25668–25679. <https://doi.org/10.1021/acs.jpcc.9b06805>.

(24) Righi, G.; Anderlini, L.; Magri, R. Reduced Cerium Configurations in CeO₂/Ag Inverse Catalysis. *Materials Letters* **2019**, 126935. <https://doi.org/10.1016/j.matlet.2019.126935>.

(25) Ševčíková, K.; Nehasil, V.; Vorokhta, M.; Haviar, S.; Matolín, V.; Matolínová, I.; Mašek, K.; Píš, I.; Kobayashi, K.; Kobata, M.; Nagata, T.; Matsushita, Y.; Yoshikawa, H. Altering Properties of Cerium Oxide Thin Films by Rh Doping. *Materials Research Bulletin* **2015**, *67*, 5–13.
<https://doi.org/10.1016/j.materresbull.2015.02.059>.

(26) Wang, X.; Rodriguez, J. A.; Hanson, J. C.; Gamarra, D.; Martínez-Arias, A.; Fernández-García, M. Unusual Physical and Chemical Properties of Cu in Ce_{1-x}Cu_xO₂ Oxides. *J. Phys. Chem. B* **2005**, *109* (42), 19595–19603. <https://doi.org/10.1021/jp051970h>.

(27) Nolan, M. Enhanced Oxygen Vacancy Formation in Ceria (111) and (110) Surfaces Doped with Divalent Cations. *J. Mater. Chem.* **2011**, *21* (25), 9160–9168. <https://doi.org/10.1039/C1JM11238D>.

(28) Hu, Z.; Li, B.; Sun, X.; Metiu, H. Chemistry of Doped Oxides: The Activation of Surface Oxygen and the Chemical Compensation Effect. *J. Phys. Chem. C* **2011**, *115* (7), 3065–3074.
<https://doi.org/10.1021/jp110333z>.

(29) Shapovalov, V.; Metiu, H. Catalysis by Doped Oxides: CO Oxidation by Au/Ce_{1-x}O₂. *Journal of Catalysis* **2007**, *245* (1), 205–214. <https://doi.org/10.1016/j.jcat.2006.10.009>.

- (30) Fernández-Torre, D.; Carrasco, J.; Ganduglia-Pirovano, M. V.; Pérez, R. Hydrogen Activation, Diffusion, and Clustering on CeO₂ (111): A DFT+ U Study. *The Journal of chemical physics* **2014**, *141* (1), 14703. <https://doi.org/10.1063/1.4885546>.
- (31) García-Melchor, M.; López, N. Homolytic Products from Heterolytic Paths in H₂ Dissociation on Metal Oxides: The Example of CeO₂. *The Journal of Physical Chemistry C* **2014**, *118* (20), 10921–10926. <https://doi.org/10.1021/jp502309r>.
- (32) Negreiros, F. R.; Camellone, M. F.; Fabris, S. Effects of Thermal Fluctuations on the Hydroxylation and Reduction of Ceria Surfaces by Molecular H₂. *The Journal of Physical Chemistry C* **2015**, *119* (37), 21567–21573.
- (33) Vicario, G.; Balducci, G.; Fabris, S.; de Gironcoli, S.; Baroni, S. Interaction of Hydrogen with Cerium Oxide Surfaces: A Quantum Mechanical Computational Study. *J. Phys. Chem. B* **2006**, *110* (39), 19380–19385. <https://doi.org/10.1021/jp061375v>.
- (34) Lykhach, Y.; Figueroba, A.; Camellone, M. F.; Neitzel, A.; Skála, T.; Negreiros, F. R.; Vorokhta, M.; Tsud, N.; Prince, K. C.; Fabris, S.; Neyman, K. M.; Matolín, V.; Libuda, J. Reactivity of Atomically Dispersed Pt₂⁺ Species towards H₂: Model Pt–CeO₂ Fuel Cell Catalyst. *Phys. Chem. Chem. Phys.* **2016**, *18* (11), 7672–7679. <https://doi.org/10.1039/C6CP00627B>.
- (35) Skála, T.; Šutara, F.; Prince, K. C.; Matolín, V. Cerium Oxide Stoichiometry Alteration via Sn Deposition: Influence of Temperature. *Journal of Electron Spectroscopy and Related Phenomena* **2009**, *169* (1), 20–25. <https://doi.org/10.1016/j.elspec.2008.10.003>.
- (36) Skála, T.; Šutara, F.; Škoda, M.; Prince, K. C.; Matolín, V. Palladium Interaction with CeO₂, Sn–Ce–O and Ga–Ce–O Layers. *Journal of Physics: Condensed Matter* **2008**, *21* (5), 055005. <https://doi.org/10.1088/0953-8984/21/5/055005>.
- (37) Horcas, I.; Fernández, R.; Gómez-Rodríguez, J. M.; Colchero, J.; Gómez-Herrero, J.; Baro, A. M. WSXM: A Software for Scanning Probe Microscopy and a Tool for Nanotechnology. *Review of Scientific Instruments* **2007**, *78* (1), 013705. <https://doi.org/10.1063/1.2432410>.
- (38) Perdew, J. P.; Burke, K.; Ernzerhof, M. Generalized Gradient Approximation Made Simple [Phys. Rev. Lett. *77*, 3865 (1996)]. *Phys. Rev. Lett.* **1997**, *78* (7), 1396. <https://doi.org/10.1103/PhysRevLett.78.1396>.
- (39) Giannozzi, P.; Baroni, S.; Bonini, N.; Calandra, M.; Car, R.; Cavazzoni, C.; Ceresoli, D.; Chiarotti, G. L.; Cococcioni, M.; Dabo, I.; Dal Corso, A.; de Gironcoli, S.; Fabris, S.; Fratesi, G.; Gebauer, R.; Gerstmann, U.; Gougoussis, C.; Kokalj, A.; Lazzeri, M.; Martin-Samos, L.; Marzari, N.; Mauri, F.; Mazzarello, R.; Paolini, S.; Pasquarello, A.; Paulatto, L.; Sbraccia, C.; Scandolo, S.; Sclauzero, G.; Seitsonen, A. P.; Smogunov, A.; Umari, P.; and Wentzcovitch, R. M. . QUANTUM ESPRESSO: A Modular and Open-Source Software Project for Quantum Simulations of Materials. *Journal of physics: Condensed matter* **2009**, *21* (39), 395502.
- (40) Giannozzi, P.; Andreussi, O.; Brumme, T.; Bunau, O.; Nardelli, M. B.; Calandra, M.; Car, R.; Cavazzoni, C.; Ceresoli, D.; Cococcioni, M.; Colonna, N.; Carnimeo, I.; Corso, A. D.; de Gironcoli, S.; Delugas, P.; Jr, R. A. D.; Ferretti, A.; Floris, A.; Fratesi, G.; Fugallo, G.; Gebauer, R.; Gerstmann, U.; Giustino, F.; Gorni, T.; Jia, J.; Kawamura, M.; Ko, H.-Y.; Kokalj, A.; Küçükbenli, E.; Lazzeri, M.; Marsili, M.; Marzari, N.; Mauri, F.; Nguyen, N. L.; Nguyen, H.-V.; Otero-de-la-Roza, A.; Paulatto, L.; Poncé, S.; Rocca, D.; Sabatini, R.; Santra, B.; Schlipf, M.; Seitsonen, A. P.; Smogunov, A.; Timrov, I.; Thonhauser, T.; Umari, P.; Vast, N.; Wu, X.; Baroni, S. Advanced Capabilities for Materials Modelling with QUANTUM ESPRESSO. *Journal of Physics: Condensed Matter* **2017**, *29* (46), 465901.

- (41) Vanderbilt, D. Soft Self-Consistent Pseudopotentials in a Generalized Eigenvalue Formalism. *Phys. Rev. B* **1990**, *41* (11), 7892–7895. <https://doi.org/10.1103/PhysRevB.41.7892>.
- (42) Cococcioni, M.; de Gironcoli, S. Linear Response Approach to the Calculation of the Effective Interaction Parameters in the LDA+U Method. *Phys. Rev. B* **2005**, *71* (3), 35105. <https://doi.org/10.1103/PhysRevB.71.035105>.
- (43) Monkhorst, H. J.; Pack, J. D. Special Points for Brillouin-Zone Integrations. *Phys. Rev. B* **1976**, *13* (12), 5188–5192. <https://doi.org/10.1103/PhysRevB.13.5188>.
- (44) Eyring, L. *Handbook on the Physics and Chemistry of Rare Earth*; North-Holland, Amsterdam, 1979; Vol. 3.
- (45) Loschen, C.; Carrasco, J.; Neyman, K. M.; Illas, F. First-Principles LDA+U and GGA+U Study of Cerium Oxides: Dependence on the Effective U Parameter. *Phys. Rev. B* **2007**, *75* (3), 035115. <https://doi.org/10.1103/PhysRevB.75.035115>.
- (46) Graciani, J.; Márquez, A. M.; Plata, J. J.; Ortega, Y.; Hernández, N. C.; Meyer, A.; Zicovich-Wilson, C. M.; Sanz, J. Fdez. Comparative Study on the Performance of Hybrid DFT Functionals in Highly Correlated Oxides: The Case of CeO₂ and Ce₂O₃. *J. Chem. Theory Comput.* **2011**, *7* (1), 56–65. <https://doi.org/10.1021/ct100430q>.
- (47) Xie, P.; Pu, T.; Nie, A.; Hwang, S.; Purdy, S. C.; Yu, W.; Su, D.; Miller, J. T.; Wang, C. Nanoceria-Supported Single-Atom Platinum Catalysts for Direct Methane Conversion. *ACS Catalysis* **2018**, *8* (5), 4044–4048. <https://doi.org/10.1021/acscatal.8b00004>.
- (48) Henkelman, G.; Uberuaga, B. P.; Jónsson, H. A Climbing Image Nudged Elastic Band Method for Finding Saddle Points and Minimum Energy Paths. *The Journal of chemical physics* **2000**, *113* (22), 9901–9904.
- (49) Fernández-Torre, D.; Carrasco, J.; Ganduglia-Pirovano, M. V.; Pérez, R. Hydrogen Activation, Diffusion, and Clustering on CeO₂ (111): A DFT+ U Study. *The Journal of chemical physics* **2014**, *141* (1), 14703.
- (50) Bader, R. F. W. *Atoms in Molecules*; Wiley Online Library, 1990.
- (51) Naumkin, A. V.; Kraut-Vass, A.; Gaarenstroom, S. W.; Powell, C. J. NIST X-Ray Photoelectron Spectroscopy Database, Version 4.1. *National Institute of Standards and Technology: Gaithersburg* **2012**.
- (52) Gaarenstroom, S. W.; Winograd, N. Initial and Final State Effects in the ESCA Spectra of Cadmium and Silver Oxides. *The Journal of Chemical Physics* **1977**, *67* (8), 3500–3506. <https://doi.org/10.1063/1.435347>.
- (53) Benedetti, S.; Nilius, N.; Valeri, S.; Tosoni, S.; Albanese, E.; Pacchioni, G. Dopant-Induced Diffusion Processes at Metal–Oxide Interfaces Studied for Iron- and Chromium-Doped MgO/Mo(001) Model Systems. *J. Phys. Chem. C* **2016**, *120* (25), 13604–13609. <https://doi.org/10.1021/acs.jpcc.6b04182>.
- (54) Matolín, V.; Matolínová, I.; Dvořák, F.; Johánek, V.; Mysliveček, J.; Prince, K. C.; Skála, T.; Stetsovykh, O.; Tsud, N.; Václavů, M.; Šmíd, B. Water Interaction with CeO₂(111)/Cu(111) Model Catalyst Surface. *Catalysis Today* **2012**, *181* (1), 124–132. <https://doi.org/10.1016/j.cattod.2011.05.032>.
- (55) Mullins, D. R.; Albrecht, P. M.; Chen, T.-L.; Calaza, F. C.; Biegalski, M. D.; Christen, H. M.; Overbury, S. H. Water Dissociation on CeO₂(100) and CeO₂(111) Thin Films. *J. Phys. Chem. C* **2012**, *116*

(36), 19419–19428. <https://doi.org/10.1021/jp306444h>.

(56) Chen, B.; Ma, Y.; Ding, L.; Xu, L.; Wu, Z.; Yuan, Q.; Huang, W. Reactivity of Hydroxyls and Water on a CeO₂(111) Thin Film Surface: The Role of Oxygen Vacancy. *J. Phys. Chem. C* **2013**, *117* (11), 5800–5810. <https://doi.org/10.1021/jp312406f>.

(57) Ganduglia-Pirovano, M. V.; Da Silva, J. L. F.; Sauer, J. Density-Functional Calculations of the Structure of near-Surface Oxygen Vacancies and Electron Localization on CeO₂ (111). *Physical review letters* **2009**, *102* (2), 26101.

(58) Fabris, S.; Vicario, G.; Balducci, G.; de Gironcoli, S.; Baroni, S. Electronic and Atomistic Structures of Clean and Reduced Ceria Surfaces. *The Journal of Physical Chemistry B* **2005**, *109* (48), 22860–22867.

(59) McFarland, E. W.; Metiu, H. Catalysis by Doped Oxides. *Chemical reviews* **2013**, *113* (6), 4391–4427.

TOC

